

Generation of high-power, tunable terahertz radiation from laser interaction with a relativistic electron beam

Zhen Zhang,^{*} Lixin Yan, Yingchao Du, Wenhui Huang, and Chuanxiang Tang
Department of Engineering Physics, Tsinghua University, Beijing 100084, China

Zhirong Huang[†]

SLAC National Accelerator Laboratory, Menlo Park, California 94025, USA

(Received 6 February 2017; published 5 May 2017)

We propose a method based on the slice energy spread modulation to generate strong subpicosecond density bunching in high-intensity relativistic electron beams. A laser pulse with periodic intensity envelope is used to modulate the slice energy spread of the electron beam, which can then be converted into density modulation after a dispersive section. It is found that the double-horn slice energy distribution of the electron beam induced by the laser modulation is very effective to increase the density bunching. Since the modulation is performed on a relativistic electron beam, the process does not suffer from strong space charge force or coupling between phase spaces, so that it is straightforward to preserve the beam quality for terahertz (THz) radiation and other applications. We show in both theory and simulations that the tunable radiation from the beam can cover the frequency range of 1–10 THz with high power and narrow-band spectra.

DOI: [10.1103/PhysRevAccelBeams.20.050701](https://doi.org/10.1103/PhysRevAccelBeams.20.050701)

I. INTRODUCTION

High-brightness electron beams have been used to drive free-electron lasers (FELs) [1–3], high-intensity terahertz (THz) radiation [4,5], advanced accelerators [6–8] and beyond. The precise manipulation of the beam phase-space distribution is often desired to advance the development in the above-mentioned fields. Recently, there has been great interest in the generation and control of high frequency structure in the current profile of relativistic electron beams. The bunched beam at picosecond (ps) and sub-ps scale can be used to produce intense narrow-band THz radiation [5,9] and resonant wakefield excitation [10–13]. Besides, in FELs, sub-ps bunched beams have been applied to generate multicolor x rays [14] based on the sideband effect [15].

There are several methods proposed and studied for the generation of ps and sub-ps bunching in electron beams, including exchanging transverse modulation to longitudinal distribution [16,17], direct modulating the drive laser [18–21] and converting wakefield induced energy modulation to density bunching [22–24]. As the development of the state-of-the-art laser technologies, laser-based manipulation of the electron beam has been implemented widely. An external-injected laser pulse

which copropagates with the electron beam inside an undulator can create energy modulation on the scale of the laser wavelength. The energy modulation can be converted into density modulation by letting the beam pass through a longitudinally dispersive element, e.g., a magnetic chicane. However, the typical laser wavelength is usually ~ 800 nm, which is much shorter than the THz wavelength. In this case, the concept of difference frequency can be used to approach THz range with two wavelengths of energy modulation in two separated undulator sections [25–27].

For the laser-based modulation method, since it is performed directly on a relativistic electron beam, the process will not suffer from the strong space charge force or coupling between transverse and longitudinal phase spaces, which is critical to preserve the beam quality for further applications. For example, in resonant wakefield excitation, the transverse focus size of the electron beam needs to match the plasma density [16], which puts a challenging constraint on the transverse normalized emittance.

In this paper, we propose a method based on the slice energy spread modulation (SESM), rather than energy modulation, to generate sub-ps density bunching in a relativistic electron beam. The slice energy spread of the beam will be modulated in a laser heater [28,29] if the laser intensity envelope varies periodically. The laser heater has been used widely in the FEL facilities [30–33]. Then after a dispersive section, strong density bunching can be obtained whose wavelength depends on the scale of laser envelope variation, not the laser wavelength. Similar methods have been adopted to generate THz radiation in a storage ring [5]

^{*}zhen-zhang12@mails.tsinghua.edu.cn

[†]zrh@slac.stanford.edu

Published by the American Physical Society under the terms of the Creative Commons Attribution 4.0 International license. Further distribution of this work must maintain attribution to the author(s) and the published article's title, journal citation, and DOI.

and multicolor x rays [14]. In this paper, we present detailed theoretical analysis on the conversion from SESM to density bunching and compare it with simulation results. We will also provide an example to produce tunable intense narrow-band THz radiation ranging from 1 to 10 THz. This method is well suited with the configuration of linear accelerator facilities and is of great potential in applications.

This paper is organized as follows. In Sec. II, detailed theoretical analysis on the conversion from SESM to density bunching is presented. It is found that the double-horn slice energy distribution from the laser modulation will help increase the available bunching factor. In Sec. III, we propose a dedicated beam line to generate intense narrow-band THz radiation based on the SESM method. Simulations are performed to demonstrate the tunable bunching frequency. Some discussions about the advantages and requirements of the proposed method will be presented in Sec. IV. Lastly, we will give a short summary in Sec. V.

II. THEORETICAL ANALYSIS

Let us assume the initial beam is uniform in current, but has a Gaussian slice energy spread $\sigma_\delta(z_0)$ that is a function of the longitudinal coordinate z_0 within the beam. The distribution can be written as

$$f_0(\delta_0, z_0) = \frac{I_0}{\sqrt{2\pi}\sigma_\delta(z_0)} \exp\left[-\frac{\delta_0^2}{2\sigma_\delta(z_0)^2}\right], \quad (1)$$

where δ_0 is the relative energy deviation and I_0 is the beam current. Due to the laser modulation, the slice energy spread is assumed to be

$$\sigma_\delta(z_0) = \bar{\sigma}[1 + A \sin(k_0 z_0)], \quad (2)$$

where $\bar{\sigma}$ is the average rms slice energy spread and $0 < A < 1$ is the relative modulation depth. The longitudinal phase space is not uniform but integration over δ_0 yields uniform current I_0 .

An energy chirp is added in the following linac section by $\delta = \delta_0 + h z_0$, and then the longitudinal dispersion occurs in a magnetic chicane as

$$z = z_0 + R_{56}\delta = z_0 + R_{56}(\delta_0 + h z_0). \quad (3)$$

Here we ignore the scale of relative energy spread due to the change of beam average energy, which can be absorbed into other parameters. The density modulation appears after the chicane with the bunching factor as follows:

$$b(k) = \frac{1}{I_0} \int d\delta dz e^{-ikz} f(\delta, z). \quad (4)$$

Using the Liouville theorem that $f(\delta, z)d\delta dz = f_0(\delta_0, z_0)d\delta_0 dz_0$ and making a change of variable from δ_0 to $\eta = \delta_0/[1 + A \sin(k_0 z_0)]$, we obtain

$$\begin{aligned} b(k) &= \int d\delta_0 dz_0 e^{-ik(1+hR_{56})z_0 - ikR_{56}\delta_0} \frac{1}{\sqrt{2\pi}\sigma_\delta(z_0)} \exp\left[-\frac{\delta^2}{2\sigma_\delta(z)^2}\right] \\ &= \int d\eta dz_0 e^{-ik(1+hR_{56})z_0 - ikR_{56}\eta[1+A \sin(k_0 z_0)]} \frac{1}{\sqrt{2\pi}\bar{\sigma}} \exp\left[-\frac{\eta^2}{2\bar{\sigma}^2}\right] \\ &= \frac{1}{\sqrt{2\pi}\bar{\sigma}} \int d\eta \exp\left[-ikR_{56}\eta - \frac{\eta^2}{2\bar{\sigma}^2}\right] \int dz_0 e^{-ik(1+hR_{56})z_0} \sum_n J_n(kR_{56}\eta A) e^{-ink_0 z_0}. \end{aligned} \quad (5)$$

Integration over z_0 yields nonvanishing bunching at the wave number $k_n = nk_0/(1 + hR_{56})$ with the bunching factor

$$b_n = \frac{(-1)^n}{\sqrt{2\pi}\bar{\sigma}} \int d\eta J_n(k_n R_{56} A \eta) e^{-ik_n R_{56} \eta - \frac{\eta^2}{2\bar{\sigma}^2}}. \quad (6)$$

Numerical calculation of Eq. (6) can be used to find the exact bunching factor and current distribution.

Here we focus only on the fundamental modulation wave number $k_1 = k_0/(1 + hR_{56})$, the bunching factor b_1 is plotted with a solid line for different $k_1 R_{56} \sigma_0$ in Fig. 1. The expression of b_1 can be simplified if we approximate $J_1(x) \approx a \sin(bx)$ for $|x| < 3$ with $a = 0.58$, $b = 0.85$, then

$$b_1 = \frac{a}{2} \left[e^{-\frac{k_1^2 R_{56}^2 \bar{\sigma}^2 (1-bA)^2}{2}} - e^{-\frac{k_1^2 R_{56}^2 \bar{\sigma}^2 (1+bA)^2}{2}} \right]. \quad (7)$$

The optimal chicane setting to achieve the largest bunching factor is to satisfy $|k_1 R_{56} \bar{\sigma}| \approx \sqrt{2 + 0.5A^2}$, and the maximum bunching factor is ~ 0.27 .

It should be noted that there is an assumption for the above derivations that the beam has a Gaussian slice energy distribution. This assumption, however, is not always true if we use a laser heater to modulate the beam's slice energy spread. In Ref. [29] it is found that when the laser size is much larger than the electron beam size, the resulting energy profile is a double-horn distribution, which will not

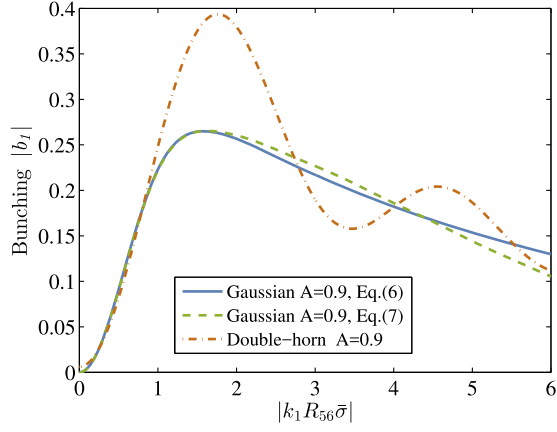


FIG. 1. Bunching factor evolution versus $k_1 R_{56} \bar{\sigma}$ with $A = 0.9$ and different slice energy distributions: (solid line) Gaussian distribution, (dashed line) Gaussian distribution but the bunching factor is calculated by Eq. (7) and (dotted line) double-horn distribution from laser heater.

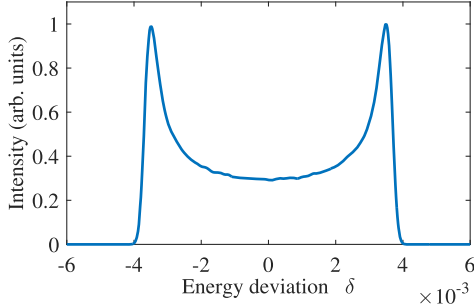


FIG. 2. Double-horn slice energy distribution of the electron beam when the laser spot size is much larger than the beam size in the laser heater. The detailed parameters can be found in Table I.

contribute much to suppress the instability. Figure 2 shows an example of double-horn distribution of the beam slice energy. The detailed parameter settings can be seen in Table I in the following sections. However, with the purpose to increase the density bunching, we find that the double-horn energy distribution is more effective to increase the bunching factor in this study.

Assuming the laser spot size is larger than the beam size and the laser power profile has the form $\sqrt{P_L(s)} = \sqrt{\bar{P}}[1 + B \cos(k_0 s)]$, the energy modulation in the laser heater can be written as

$$\delta_f = \delta_i + \Delta[1 + B \cos(k_0 s)], \quad (8)$$

with initial and final relative energy deviation δ_i , δ_f and energy modulation amplitude Δ . The full expression for Δ can be found, e.g. in Ref. [29]. To compare with Gaussian distribution, we define an effective modulation depth

TABLE I. Beam parameters before the modulator in the simulations.

Parameter	Value	Units
Electron beam		
Charge	500	pC
Beam energy	135	MeV
Current profile	flattop	...
Bunch length	~ 10	ps
Intrinsic slice energy spread	10^{-4}	...
Normalized emittance	1	mm-mrad
rms beam size	200	μm
Modulator		
Laser wavelength	800	nm
Undulator period	5	cm
Period number	10	...
Laser waist size	1.5	mm
Laser stacking separation	0.5 (0.25 ^a)	ps
rms laser pulse length	60 (30)	fs
Laser power	1 (0.26)	GW

^aThe numbers in brackets are the parameters for the 4 THz case.

$$A = \frac{\sqrt{\Delta^2(1+B)^2 + \sigma_0^2} - \sqrt{\Delta^2(1-B)^2 + \sigma_0^2}}{\sqrt{\Delta^2(1+B)^2 + \sigma_0^2} + \sqrt{\Delta^2(1-B)^2 + \sigma_0^2}} \approx 1 - \frac{2\sqrt{\Delta^2(1-B)^2 + \sigma_0^2}}{\Delta(1+B)}, \quad (9)$$

where σ_0 is the initial rms energy spread. The approximation above adopts the assumptions that $\Delta \gg \sigma_0$ and $B \approx 1$. When $\Delta/\sigma_0 = 10$, $B = 1$, the modulation depth $A = 0.9$. Numerical calculation results of the bunching factor for

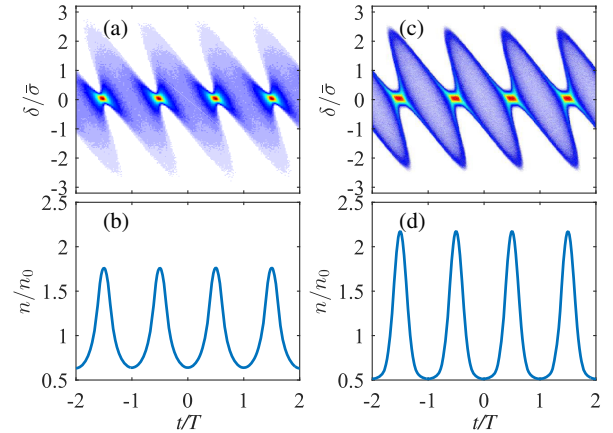


FIG. 3. Longitudinal phase spaces and the corresponding density profile with the largest bunching factor in the two different energy distributions with the same modulation depth $A = 0.9$. The energy is scaled by the rms energy spread and the time is scaled by the period of the bunching. (a) and (b) are Gaussian energy distribution and (c) and (d) are double-horn distribution.

different R_{56} are presented in Fig. 1. The optimal R_{56} is similar with the Gaussian case, but the maximum bunching factor is increased to ~ 0.4 with the optimal condition $|k_1 R_{56} \bar{\sigma}| \approx 1.75$.

The longitudinal phase spaces and the corresponding density profiles of the electron beam that give the largest bunching factor in both cases are presented in Fig. 3. The physical meaning of $k_1 R_{56} \bar{\sigma}$ denotes the rotation angle of the phase space. As the increase of the R_{56} , the phase space begins to rotate counterclockwise and the projected density profile will have peaks and valleys. At a certain angle, the bunching factor reaches its largest value. The similar rotation angle of the two phase spaces in Fig. 3 verifies that they both achieve optimal bunching at similar $k_1 R_{56} \bar{\sigma}$. In order to optimize the bunching for different parts of the beam at the same R_{56} , the modulation depth and the average slice energy spread needs to be uniform over the whole beam. In the double-horn distribution case, the peaks in density profile are higher and sharper, resulting in a larger bunching factor.

III. THz RADIATION GENERATION

From the theoretical analysis in the previous section, the proposed method using SESM can produce strong density bunching in a relativistic electron beam with a bunching factor about 0.4. Based on this method, we propose a dedicated beam line design for tunable intense narrow-band THz radiation generation in Fig. 4, which can be implemented in most x-ray FEL facilities or dedicated small THz facilities. The electron beam is generated and accelerated by the gun and the first section of linac before it goes into the modulator. In a typical laser heater design, the undulator is located in the center of a chicane to smear out the laser-induced energy modulation. However, we do not have to do this since the density bunching scale of interest here is much larger than the laser wavelength. The drive laser of the gun and the modulation laser can share the same laser system to make the synchronization between electron beam and laser easier. After the modulator, the beam will pass through the second section of linac with $\pm 90^\circ$ off-crest acceleration phase to add the energy chirp for THz frequency control without net energy gain. The final chicane is set at optimal value to convert the SESM to density modulation and the radiation frequency is varied by tuning the energy chirp from the second linac. In practice,

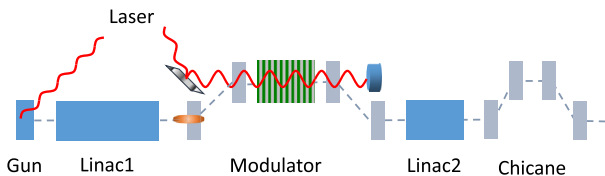


FIG. 4. Schematic layout of the proposed beam line for tunable intense narrow-band THz radiation generation.

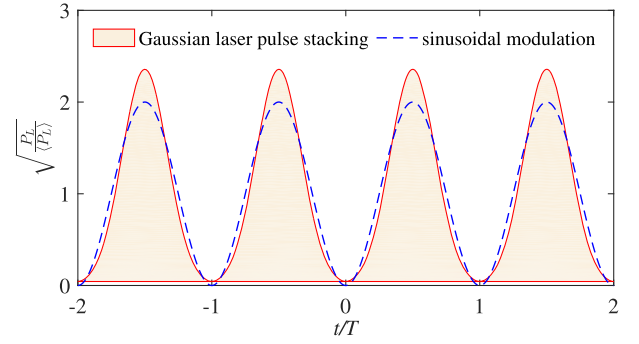


FIG. 5. Laser pulse train distribution. The dashed line denotes the full sinusoidal modulation profile for comparison.

the average slice energy spread $\bar{\sigma}$ can be calculated after removing the existing energy chirp.

The laser pulse with oscillating power envelop can be generated by chirped pulse beating [34] or pulse stacking techniques. In the previous work [5,14], the lasers are both modulated by the first method. Here we discuss the pulse stacking method with α -BBO birefringent crystals [35,36]. Taking 2 THz density modulation as an example, we need to stack the laser pulse with a uniform separation $T = 0.5$ ps. Using crystals with decreasing thickness and assuming the initial laser pulse is of Gaussian profile with rms width 60 fs, the numerical simulation of the stacked laser pulse train is shown in Fig. 5. For comparison, we also plot the sinusoidal modulation of the same period with full modulation depth (the intensity minimum along the laser pulse is zero).

We use the particle tracking code ELEGANT [37] to simulate the laser modulation and beam dynamics with wakefield and longitudinal space charge effects. For similarity, the simulation starts from the end of the first linac with the beam and modulator parameters listed in Table I, which is realistic and readily available from the injector of many FEL facilities. The current profile of the electron beam is ~ 10 ps flop-top distribution. The laser envelop modulation period is 2 and 4 THz, respectively. The waist size of the laser in the modulator is 1.5 mm, much larger than the electron beam size to generate double-horn slice energy distribution as discussed in the previous section.

As obtained from the theory, the bunching factor optimizes when $|k_1 R_{56} \bar{\sigma}| \approx 1.75$. For one certain frequency of density bunching, we need to match the R_{56} and the average slice energy spread after the modulator. The energy spread is controlled by the laser power. For the 2 THz case, the laser peak power is 1 GW and the average energy spread after modulator is 190 keV (1.4×10^{-3}), leading to the optimal $R_{56} = -29.4$ mm. To verify the theoretical prediction, we turn off the Linac2 and scan the R_{56} of the chicane in the simulation. The bunching factor at the fundamental frequency and the peak current are presented in Fig. 6. The optimal R_{56} with the largest bunching factor

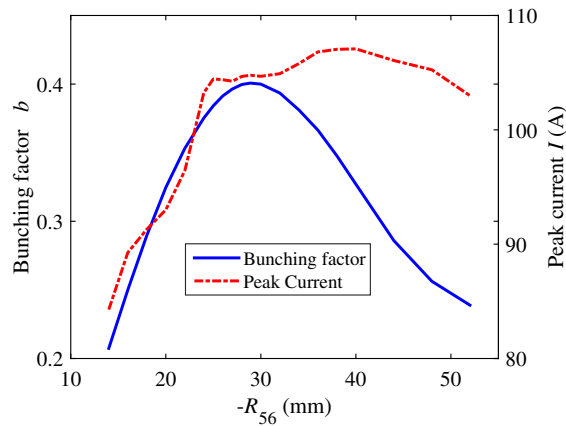


FIG. 6. Bunching factor at 2 THz and peak current of the electron beam for different R_{56} of the chicane. The laser power is fixed at 1 GW and zero energy chirp is added onto the beam.

at 2 THz is -29 mm, which agrees well with the theory prediction. The longitudinal phase space and beam current profile at $R_{56} = -29$ mm are given in Fig. 7. As the increase of R_{56} from the optimal value, the bunching factor decreases while the peak current keep almost constant. In the conversion from SESM to density modulation, as the rotation of the phase space the current spikes become narrower and sharper and keep similar peak value, indicating more harmonic components. The double-horn distribution also helps maintain the peak current for different R_{56} . The residual energy chirp on the beam is due to the linac wakefield and longitudinal space charge effects, which can be compensated by the linac section with off-crest acceleration.

The bunching frequency can be controlled by the induced energy chirp from the Linac2 (an S-band acceleration structure in the simulation) before the chicane. As the bunching frequency changes, we need to vary R_{56} and laser power to maintain the bunching factor. If we fix the laser power at 1 GW, the R_{56} needs to be varied as shown in Fig. 8. The bunching frequency can be varied from 1 to

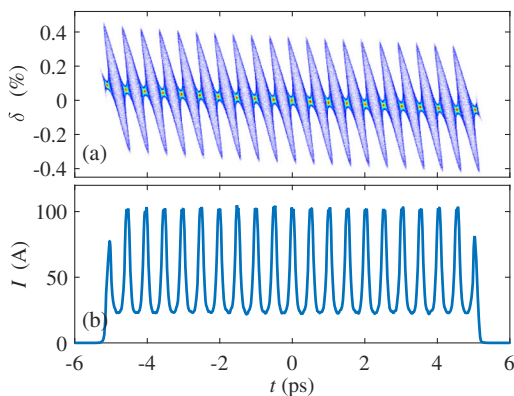


FIG. 7. Phase space of the electron beam with largest bunching factor. $R_{56} = -29$ mm and laser power 1 GW.

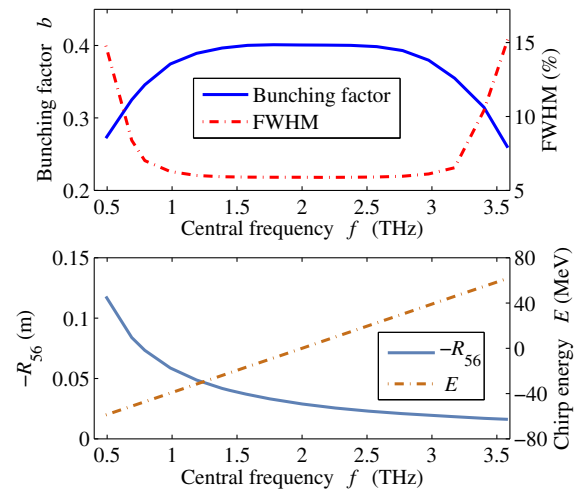


FIG. 8. Bunching factor and the FWHM of the bunching spectra for different radiation frequency by matching the R_{56} and chirp energy. The laser power is fixed at 1 GW.

3 THz with almost constant bunching factor 0.4. We also show the full width of half maximum (FWHM) of the bunching spectra and the requirement for the chirp energy of Linac2. The degradation of the bunching factor and the increase of the spectra bandwidth are both due to the nonlinear effects during the beam compression or stretching.

In addition, we can also choose to vary the laser power and fix the R_{56} . Figure 9 presents the results of bunching factor, FWHM, required laser and chirp energy for different frequencies, which are similar with the results of varying R_{56} . In practice, we can vary both R_{56} and laser power to optimize the bunching factor for different frequencies based on the availability of the beam line.

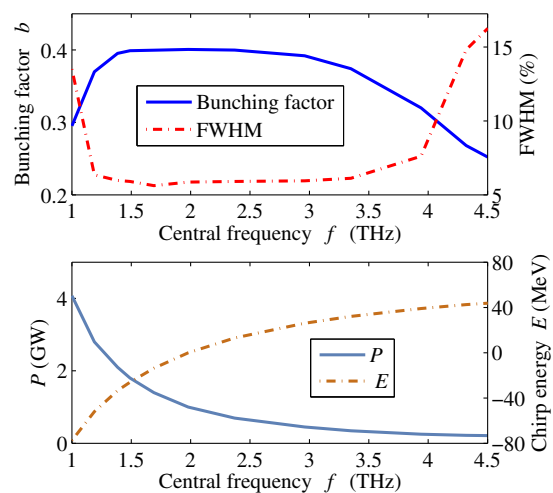


FIG. 9. Bunching factor and the FWHM of the bunching spectra for different radiation frequency by matching the laser power and chirp energy. The R_{56} is fixed at -29 mm.

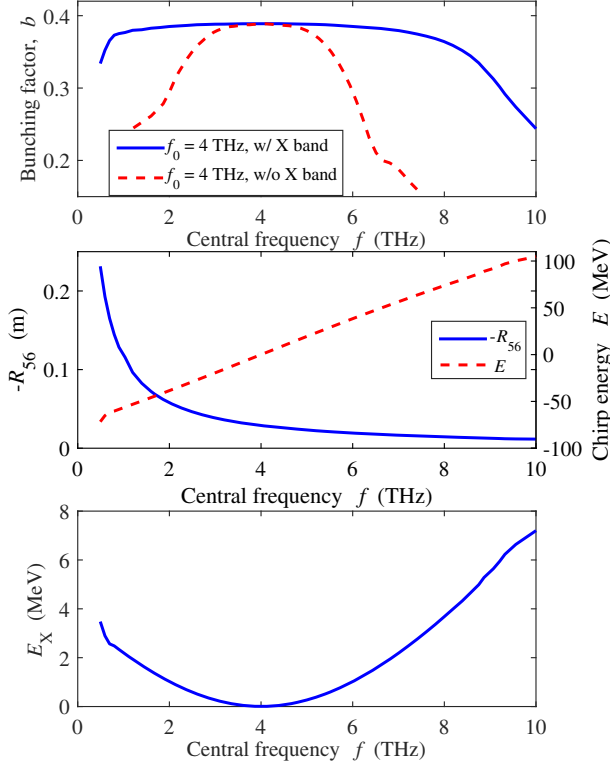


FIG. 10. (top) Bunching factor for different radiation frequency with and without the X-band cavity. (middle) The requirements for R_{56} and chirp energy. (bottom) The requirement for energy gain of the X-band cavity.

Lastly, we present some examples of 4 THz density modulation simulations. As the frequency is increased by a factor of 2, the laser power is decreased to 0.26 GW to meet the optimal condition with $R_{56} = -29$ mm. By varying R_{56} , the bunching frequency can be varied between 2 to 6 THz with a bunching factor larger than 0.3, as shown in Fig. 10. However, if we add a harmonic rf cavity that decelerates the beam at -180° before the chicane to compensate for the nonlinear effects during compression, the frequency range of the modulation can be extended significantly. In Fig. 10, we give the requirements for R_{56} , chirp energy, and especially the maximum energy gain of a 4th-harmonic (X-band) cavity to vary bunching frequency. With the help of chirp compensation from the X-band cavity (e.g. [38]), the bunching frequency range is extended from 1 to ~ 8 THz with the bunching factor keeping at ~ 0.38 .

Note that the bunching frequency control discussed above is to compress or stretch the electron beam. Alternatively we can also change the laser intensity modulation period directly to control the bunching frequency. As the increase of bunching frequency k_1 , the R_{56} of the chicane or (and) the laser power needs to be decreased to keep the optimal condition. Usually laser-induced energy spread should be much larger than the

initial slice energy spread to introduce enough effective modulation depth, so reducing the R_{56} of the chicane will be a better choice. Compared with the beam compression, in this method the nonlinear effects in the chicane will be smaller, which is helpful to maintain the density bunching. In addition, the number of sub-bunches in the train will become larger for higher modulation frequency, resulting in smaller bandwidth in the spectra.

IV. DISCUSSIONS

The proposed method is of great advantage in the generations of tunable narrow-band THz radiation. The bunching factor averaged over the beam can be kept around 0.4 for a wide range of frequency, covering the THz gap, by varying the beam compression and (or) the initial laser modulation period. The proposed method is robust as it is performed on a very relativistic electron beam. Since there is no strong space charge force or beam loss during the process, the beam quality can be preserved for beam matching and focusing. Assuming that the beam is focused to a small spot and the frequency cut due to finite dimensions of the target, e.g., a metallic foil, can be neglected, it is possible to estimate the THz energy emitted by this beam as

$$W = N_e^2 b^2 \frac{dW_1}{d\omega} \Delta\omega, \quad (10)$$

where b is the bunching factor, N_e is the number of electrons for coherent emission, $\frac{dW_1}{d\omega}$ is the single particle spectral power which for transition radiation is relatively flat and equal to $\frac{2}{\pi} m_e r_e c \ln \gamma$, with m_e the rest electron mass and r_e the classical electron radius. $\Delta\omega$ is the linewidth which is equal to 1 over the number of cycles in the pulse train. Although the beam charge is set at 0.5 nC in the previous simulations, there is no strict constraint on beam charge and beam repetition rate. Using 2 THz radiation as an example, the THz pulse energy emitted from 10-ps beam is shown in Fig. 11 as a function of beam charge. When the

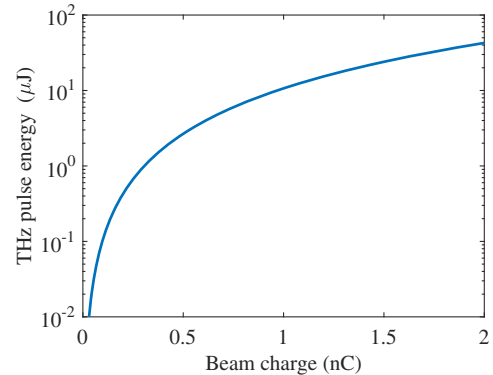


FIG. 11. THz pulse energy around 2 THz frequency in 5% bandwidth emitted from 10-ps beam for different beam charge.

charge is 2 nC, the pulse energy is up to more than 40 μJ centered around 2 THz frequency in 5% bandwidth. The spectra brightness and THz field are both significantly improved.

Finally, we note that using an undulator [9] or a dielectric tube [24,39,40] can further enhance the output THz energy to approach the mJ level. Considering the undulator radiation of 135 MeV electron beam, the undulator period is $\lambda_w = 10$ cm and helical undulator strength $K = 11.77$ to be resonant at 3 THz. The output THz energy W can be estimated as [41]

$$W = W_b \left[\frac{\pi^2 a_{\text{in}}^2}{2} \right] \left[\frac{I}{\gamma I_A} \right] \left[\frac{K^2}{1 + K^2} \right] N_w, \quad (11)$$

where W_b is the beam energy and $a_{\text{in}} = 2b$, b is the bunching factor. For $N_w = 100$ period and 2 nC beam charge, the THz pulse energy $W_0 = 1.2$ mJ. The pulse energy can be improved with further optimization.

In passing we note that our proposal does not require a linac with a photocathode rf gun. The method is also applicable for the electron beams from storage rings, energy recovery linacs or thermal-cathode injectors with higher repetition rate. The main requirement of the method is the electron beam energy needs to be ~ 100 MeV to be resonant with an optical laser. However, for electron beams with lower energies (~ 50 MeV), it is still possible to interact harmonically with the optical laser. Thus, such an intense THz source can be driven by a very compact accelerator.

V. SUMMARY

In this paper, we have proposed a method based on the slice energy spread modulation to generate strong density bunching in a relativistic electron beam, which can be used to produce intense narrow-band THz radiation. Theoretical analysis and simulations both show that with the help of double-horn slice energy spread distribution from the laser modulation, the bunching factor can reach up to 0.4 for modulation frequencies ranging from 1 to 10 THz. We also found the optimal condition involving the bunching frequency, R_{56} of the conversion section and the average slice energy spread to maximum the bunching factor. To implement this scheme in an existing x-ray FEL, very minimal hardware additions are required. The use of the laser in our proposal makes the THz signal synchronize with the optical signal and has a stable waveform. Various laser shaping techniques (e.g., Ref. [42]) can be applied to produce tailored THz waveforms for specific applications. The high spectra brightness of the radiation makes it a powerful and promising method for many applications, such as THz pump [43], THz streaking [44] and THz acceleration [45].

ACKNOWLEDGMENTS

We thank Enrico Allaria and Agostino Marinelli for very helpful discussions. This work was supported by the National Natural Science Foundation of China (NSFC Grants No. 11375097, No. 11435015 and No. 11475097) and U.S. Department of Energy Contract No. DE-AC02-76SF00515.

-
- [1] W. Ackermann, G. Asova, V. Ayvazyan, A. Azima, N. Baboi, J. Bähr, V. Balandin, B. Beutner, A. Brandt, A. Bolzmann *et al.*, Operation of a free-electron laser from the extreme ultraviolet to the water window, *Nat. Photonics* **1**, 336 (2007).
 - [2] P. Emma, R. Akre, J. Arthur, R. Bionta, C. Bostedt, J. Bozek, A. Brachmann, P. Bucksbaum, R. Coffee, F.-J. Decker *et al.*, First lasing and operation of an ångstrom-wavelength free-electron laser, *Nat. Photonics* **4**, 641 (2010).
 - [3] T. Ishikawa, H. Aoyagi, T. Asaka, Y. Asano, N. Azumi, T. Bizen, H. Ego, K. Fukami, T. Fukui, Y. Furukawa *et al.*, A compact X-ray free-electron laser emitting in the sub-ångström region, *Nat. Photonics* **6**, 540 (2012).
 - [4] G.L. Carr, M.C. Martin, W.R. McKinney, K. Jordan, G.R. Neil, and G.P. Williams, High-power terahertz radiation from relativistic electrons, *Nature (London)* **420**, 153 (2002).
 - [5] S. Bielawski, C. Evain, T. Hara, M. Hosaka, M. Katoh, S. Kimura, A. Mochihashi, M. Shimada, C. Szwej, T. Takahashi *et al.*, Tunable narrowband terahertz emission from master laser–electron beam interaction, *Nat. Phys.* **4**, 390 (2008).
 - [6] I. Blumenfeld, C. E. Clayton, F.-J. Decker, M. J. Hogan, C. Huang, R. Ischebeck, R. Iverson, C. Joshi, T. Katsouleas, N. Kirby *et al.*, Energy doubling of 42 GeV electrons in a metre-scale plasma wakefield accelerator, *Nature (London)* **445**, 741 (2007).
 - [7] M. Litos, E. Adli, W. An, C. Clarke, C. Clayton, S. Corde, J. Delahaye, R. England, A. Fisher, J. Frederico *et al.*, High-efficiency acceleration of an electron beam in a plasma wakefield accelerator, *Nature (London)* **515**, 92 (2014).
 - [8] C. Jing, A. Kanareykin, J. Power, M. Conde, Z. Yusof, and W. Gai, Observation of Enhanced Transformer Ratio in Collinear Wakefield Acceleration, *Phys. Rev. Lett.* **98**, 144801 (2007).
 - [9] A. Gover, Superradiant and stimulated-superradiant emission in prebunched electron-beam radiators. I. Formulation, *Phys. Rev. ST Accel. Beams* **8**, 030701 (2005).
 - [10] P. Chen, J. Dawson, R. W. Huff, and T. Katsouleas, Acceleration of Electrons by the Interaction of a Bunched Electron Beam with a Plasma, *Phys. Rev. Lett.* **54**, 693 (1985).
 - [11] R.D. Ruth, P. Morton, P.B. Wilson, and A. Chao, A plasma wake field accelerator, *Part. Accel.* **17**, 171 (1984).
 - [12] P. Schutt, T. Weiland, and V. Tsakanov, On the wake field acceleration using the sequence of driving bunches, in *Proceedings of the Second All-Union Conference on New Methods of Charged Particle Acceleration* (Springer, New York, 1989).

- [13] J. Power, W. Gai, A. Kanareykin, P.L. Colestock, and S. Kelley, Transformer ratio enhancement using a ramped bunch train in a collinear wakefield accelerator, *AIP Conf. Proc.* **569**, 605 (2001).
- [14] E. Roussel, E. Ferrari, E. Allaria, G. Penco, S. Di Mitri, M. Veronese, M. Danailov, D. Gauthier, and L. Giannessi, Multicolor High-Gain Free-Electron Laser Driven by Seeded Microbunching Instability, *Phys. Rev. Lett.* **115**, 214801 (2015).
- [15] Z. Zhang, R. Lindberg, W.M. Fawley, Z. Huang, J. Krzywinski, A. Lutman, G. Marcus, and A. Marinelli, Microbunching-instability-induced sidebands in a seeded free-electron laser, *Phys. Rev. Accel. Beams* **19**, 050701 (2016).
- [16] P. Muggli, V. Yakimenko, M. Babzien, E. Kallos, and K. Kusche, Generation of Trains of Electron Microbunches with Adjustable Subpicosecond Spacing, *Phys. Rev. Lett.* **101**, 054801 (2008).
- [17] Y.-E. Sun, P. Piot, A. Johnson, A. Lumpkin, T. Maxwell, J. Ruan, and R. Thurman-Keup, Tunable Subpicosecond Electron-Bunch-Train Generation Using a Transverse-To-Longitudinal Phase-Space Exchange Technique, *Phys. Rev. Lett.* **105**, 234801 (2010).
- [18] Y. Shen, X. Yang, G. Carr, Y. Hidaka, J. B. Murphy, and X. Wang, Tunable Few-Cycle and Multicycle Coherent Terahertz Radiation from Relativistic Electrons, *Phys. Rev. Lett.* **107**, 204801 (2011).
- [19] Y. Li and K.-J. Kim, Nonrelativistic electron bunch train for coherently enhanced terahertz radiation sources, *Appl. Phys. Lett.* **92**, 014101 (2008).
- [20] P. Musumeci, R. Li, and A. Marinelli, Nonlinear Longitudinal Space Charge Oscillations in Relativistic Electron Beams, *Phys. Rev. Lett.* **106**, 184801 (2011).
- [21] Z. Zhang, L. Yan, Y. Du, Z. Zhou, X. Su, L. Zheng, D. Wang, Q. Tian, W. Wang, J. Shi *et al.*, Tunable High-Intensity Electron Bunch Train Production Based on Nonlinear Longitudinal Space Charge Oscillation, *Phys. Rev. Lett.* **116**, 184801 (2016).
- [22] S. Antipov, C. Jing, M. Fedurin, W. Gai, A. Kanareykin, K. Kusche, P. Schoessow, V. Yakimenko, and A. Zholents, Experimental Observation of Energy Modulation in Electron Beams Passing through Terahertz Dielectric Wakefield Structures, *Phys. Rev. Lett.* **108**, 144801 (2012).
- [23] K. Bane and G. Stupakov, Terahertz radiation from a pipe with small corrugations, *Nucl. Instrum. Methods Phys. Res., Sect. A* **677**, 67 (2012).
- [24] S. Antipov, M. Babzien, C. Jing, M. Fedurin, W. Gai, A. Kanareykin, K. Kusche, V. Yakimenko, and A. Zholents, Subpicosecond Bunch Train Production for a Tunable mJ Level THz Source, *Phys. Rev. Lett.* **111**, 134802 (2013).
- [25] D. Xiang and G. Stupakov, Enhanced tunable narrow-band THz emission from laser-modulated electron beams, *Phys. Rev. ST Accel. Beams* **12**, 080701 (2009).
- [26] M. Dunning, C. Hast, E. Hemsing, K. Jobe, D. McCormick, J. Nelson, T. Raubenheimer, K. Soong, Z. Szalata, D. Walz *et al.*, Generating Periodic Terahertz Structures in a Relativistic Electron Beam through Frequency Down-Conversion of Optical Lasers, *Phys. Rev. Lett.* **109**, 074801 (2012).
- [27] Z. Wang, D. Huang, Q. Gu, Z. Zhao, and D. Xiang, Echo-enabled tunable terahertz radiation generation with a laser-modulated relativistic electron beam, *Phys. Rev. ST Accel. Beams* **17**, 090701 (2014).
- [28] E. Saldin, E. Schneidmiller, and M. Yurkov, Longitudinal space charge-driven microbunching instability in the TESLA Test Facility linac, *Nucl. Instrum. Methods Phys. Res., Sect. A* **528**, 355 (2004).
- [29] Z. Huang, M. Borland, P. Emma, J. Wu, C. Limborg, G. Stupakov, and J. Welch, Suppression of microbunching instability in the linac coherent light source, *Phys. Rev. ST Accel. Beams* **7**, 074401 (2004).
- [30] Z. Huang, A. Brachmann, F.-J. Decker, Y. Ding, D. Dowell, P. Emma, J. Frisch, S. Gilevich, G. Hays, P. Hering *et al.*, Measurements of the linac coherent light source laser heater and its impact on the x-ray free-electron laser performance, *Phys. Rev. ST Accel. Beams* **13**, 020703 (2010).
- [31] E. Ferrari, E. Allaria, W. Fawley, L. Giannessi, Z. Huang, G. Penco, and S. Spampinati, Impact of Non-Gaussian Electron Energy Heating upon the Performance of a Seeded Free-Electron Laser, *Phys. Rev. Lett.* **112**, 114802 (2014).
- [32] S. Spampinati, E. Allaria, L. Badano, S. Bassanese, S. Biedron, D. Castronovo, P. Craievich, M. Danailov, A. Demidovich, G. De Ninno *et al.*, Laser heater commissioning at an externally seeded free-electron laser, *Phys. Rev. ST Accel. Beams* **17**, 120705 (2014).
- [33] J. Lee, J.-H. Han, S. Lee, J. Hong, C. H. Kim, C. K. Min, and I. S. Ko, PAL-XFEL laser heater commissioning, *Nucl. Instrum. Methods Phys. Res., Sect. A* **843**, 39 (2017).
- [34] A. S. Weling and D. H. Auston, Novel sources and detectors for coherent tunable narrow-band terahertz radiation in free space, *J. Opt. Soc. Am. B* **13**, 2783 (1996).
- [35] P. Musumeci, J. Moody, C. Scoby, M. Gutierrez, M. Westfall, and R. Li, Capturing ultrafast structural evolutions with a single pulse of MeV electrons: Radio frequency streak camera based electron diffraction, *J. Appl. Phys.* **108**, 114513 (2010).
- [36] L.-X. Yan, J.-F. Hua, Y.-C. Du, Y.-F. Huang, Y. You, D. Wang, W.-H. Huang, and C.-X. Tang, UV pulse trains by α -BBO crystal stacking for the production of THz-rap-rate electron bunches, *J. Plasma Phys.* **78**, 429 (2012).
- [37] M. Borland, ELEGANT, Technical Report (Advanced Photon Source LS-287, 2003).
- [38] P. Emma, SLAC Report No. ILCLS-TN-01-1, 2001.
- [39] A. Cook, R. Tikhoplav, S. Y. Tochitsky, G. Travish, O. Williams, and J. Rosenzweig, Observation of Narrow-Band Terahertz Coherent Cherenkov Radiation from a Cylindrical Dielectric-Lined Waveguide, *Phys. Rev. Lett.* **103**, 095003 (2009).
- [40] G. Andonian, O. Williams, X. Wei, P. Niknejadi, E. Hemsing, J. Rosenzweig, P. Muggli, M. Babzien, M. Fedurin, K. Kusche *et al.*, Resonant excitation of coherent Cerenkov radiation in dielectric lined waveguides, *Appl. Phys. Lett.* **98**, 202901 (2011).
- [41] E. L. Saldin, E. A. Schneidmiller, and M. V. Yurkov, A simple method for the determination of the structure of ultrashort relativistic electron bunches, *Nucl. Instrum. Methods Phys. Res., Sect. A* **539**, 499 (2005).

- [42] A. Marinelli, R. Coffee, S. Vetter, P. Hering, G. West, S. Gilevich, A. Lutman, S. Li, T. Maxwell, J. Galayda *et al.*, Optical Shaping of X-Ray Free-Electron Lasers, *Phys. Rev. Lett.* **116**, 254801 (2016).
- [43] M. Liu, H. Y. Hwang, H. Tao, A. C. Strikwerda, K. Fan, G. R. Keiser, A. J. Sternbach, K. G. West, S. Kittiwatanakul, J. Lu *et al.*, Terahertz-field-induced insulator-to-metal transition in vanadium dioxide metamaterial, *Nature (London)* **487**, 345 (2012).
- [44] U. Fröhling, M. Wieland, M. Gensch, T. Gebert, B. Schütte, M. Krikunova, R. Kalms, F. Budzyn, O. Grimm, J. Rossbach *et al.*, Single-shot terahertz-field-driven X-ray streak camera, *Nat. Photonics* **3**, 523 (2009).
- [45] E. A. Nanni, W. R. Huang, K.-H. Hong, K. Ravi, A. Fallahi, G. Moriena, R. D. Miller, and F. X. Kärtner, Terahertz-driven linear electron acceleration, *Nat. Commun.* **6**, 8486 (2015).